

Chalmers Publication Library



CHALMERS

Copyright Notice IEEE

©20XX IEEE. Personal use of this material is permitted. However, permission to reprint/republish this material for advertising or promotional purposes or for creating new collective works for resale or redistribution to servers or lists, or to reuse any copyrighted component of this work in other works must be obtained from the IEEE.

(Article begins on next page)

MRC Diversity and MIMO Capacity Evaluations of Multi-Port Antennas Using Reverberation Chamber and Anechoic Chamber

Xiaoming Chen, Per-Simon Kildal, *Fellow, IEEE*, Jan Carlsson, *Member, IEEE*, and Jian Yang, *Senior Member, IEEE*

Abstract—It has been shown that diversity gains and MIMO capacity of multi-port antennas can be conveniently determined from reverberation chamber measurements. In this paper, we first present the covariance eigenvalue approach and the embedded far field function method to determine diversity gain and MIMO capacity, respectively, for arbitrary multi-port antennas. Then, we discuss the convergence of the covariance eigenvalue approach. In the end, we apply both methods to compare MRC diversity gains and MIMO capacity measured in a reverberation chamber (based on direct channel measurements) and an anechoic chamber (based on measurements of the embedded far field functions and efficiencies at all antenna ports). The comparison is performed over 2–8 GHz using a wideband multi-port antenna in two configurations. There are in general good agreements between the reverberation and anechoic chamber measurement results.

Index Terms—Anechoic chamber, MIMO capacity, MRC diversity, reverberation chamber.

I. INTRODUCTION

MULTI-ANTENNA systems have drawn considerable attention over the past decade due to the improved diversity gain [1]–[5] and multiplexing gain [6]–[9]. From the antenna point of view, both diversity gain [3] and MIMO capacity [6] are appropriate parameters for multi-port antenna characterizations in multipath environments. Due to the measurement repeatability and convenience of the reverberation chamber, it has become a popular multipath emulator [10]–[12] for measurements of multi-port antennas [13]–[18] and active MIMO terminal [19]–[21]. The reverberation chamber emulates a rich isotropic multipath (RIMP) environment, being a contrast to the well known pure Line-Of-Sight (LOS) in an anechoic environment [20].

It is shown in [14] that estimating diversity gain at 1% CDF level requires a huge amount of channel samples for convergence, which is difficult and (if possible) time-consuming to achieve for a reverberation chamber measurement. Using the theoretical CDF formula derived in [2], a fast convergent diver-

sity gain can be achieved [4], [14]. In the present paper, we use the same method to calculate the (maximum ratio combining) MRC diversity gain of multi-port antennas over a wide bandwidth. However, the approach requires distinct eigenvalues of the covariance matrix, since two identical eigenvalues result in singularity [2]. It is believed that two close eigenvalues will result in large numerical error due to the singularity. However, we show that such diversity gain estimate actually converges to the true value when any two eigenvalues approach each other. This means that this method works for arbitrary antennas when it is based on stochastic channel data from measurements in reverberation chamber. We also use this method to compare MRC diversity gain of a multi-port antenna from both reverberation and anechoic chamber measurements.

It was shown in [13] that the MIMO capacity can be readily determined from measured channels in a reverberation chamber, which intrinsically include the overall antenna effect. An alternative way of computing the MIMO capacity is to use numerically generated random channel matrices and then include the antenna effects (based on anechoic chamber measurements) in the channel matrices. Nevertheless, the far field functions are quite laborious to measure in an anechoic chamber. Preliminary results of MIMO capacity comparison of anechoic and reverberation chamber measurements were presented in [15]. However, the embedded far field function method in [15] works only for power-balanced two-port antennas. A generalized method that works for arbitrary multi-port antenna has been presented initially in [16]. However, the work of [16] is based solely on reverberation chamber measurements. As a result, the generalized method to date has not been applied to measured data. In this paper, we apply this method to anechoic chamber measurements using both power-balanced and power-unbalanced antennas, and compare the results with that measured in a reverberation chamber. Moreover, instead of comparing only ergodic capacities as in [15], we also calculate and compare the CDF of the instantaneous capacity, which allow us to examine the measured capacity in greater details. Finally, we investigate the contributions of antenna efficiencies and correlations to the diversity gain and the capacity, respectively, by combining measured antenna characteristics with simulated random channel matrices. This allows us to separately examine the effects of the antenna efficiency and correlation on the MIMO performance.

The paper is of particular interest because both reverberation chamber and anechoic chamber are being considered for standardization of over-the-air (OTA) measurements [10]–[12] for characterization of active wireless MIMO terminals.

Manuscript received March 24, 2012; revised August 19, 2012; accepted September 22, 2012. Date of publication October 09, 2012; date of current version January 30, 2013. This work was supported in part by The Swedish Governmental Agency for Innovation Systems (VINNOVA) within the VINN Excellence Center Chase and in part by NordForsk.

X. Chen, P.-S. Kildal, and J. Yang are with Chalmers University of Technology, Gothenburg, Sweden (e-mail: xiaoming.chen@chalmers.se).

J. Carlsson is with the Electronics department, SP Technical Research Institute of Sweden, Borås, Sweden.

Color versions of one or more of the figures in this paper are available online at <http://ieeexplore.ieee.org>.

Digital Object Identifier 10.1109/TAP.2012.2223442

II. FORMULATION OF MRC DIVERSITY GAIN

In this section, we first present an approach for calculations of MRC diversity gains. Then we investigate the convergence of this approach.

A. Covariance Eigenvalue Approach

Assuming an N -port diversity antenna in a Rayleigh-fading environment (e.g. a reverberation chamber), its covariance matrix is

$$\mathbf{R} = E[\mathbf{h}\mathbf{h}^H] \quad (1)$$

where \mathbf{h} is the complex baseband column-vector fading channel including overall antenna effects, the superscript H is Hermitian operator, and E is mathematical expectation. Throughout this paper, E is approximated by sample mean in all simulations and measurements. The joint probability density function (PDF) of \mathbf{h} is,

$$p(\mathbf{h}) = \frac{1}{(2\pi)^N \det(\mathbf{R})} \exp(-\mathbf{h}^H \mathbf{R}^{-1} \mathbf{h}). \quad (2)$$

The MRC output power is defined as

$$P_{MRC} = \mathbf{h}^H \mathbf{h}. \quad (3)$$

Assuming independent, identically distributed (i.i.d.) Gaussian noises with unity variance, P_{MRC} then equals in value to the instantaneous signal-to-noise ratio (SNR), denoted as γ . The characteristic function [22] of γ is

$$\phi(z) = E[\exp(jz\gamma)]. \quad (4)$$

Equation (4) can be expressed as [23]

$$\phi(z) = \frac{1}{\det(\mathbf{I} + z\mathbf{R})} = \prod_{i=1}^N \frac{1}{1 + z\lambda_i} \quad (5)$$

where λ_i denotes the i th eigenvalues of \mathbf{R} . The PDF of γ is the inverse Fourier transform of $\phi(z)$ [2],

$$p(\gamma) = \frac{1}{\prod_i \lambda_i} \sum_i \frac{\exp(-\gamma/\lambda_i)}{\prod_{k \neq i} (1/\lambda_k - 1/\lambda_i)}. \quad (6)$$

The CDF of γ can be readily derived as [2],

$$F(\gamma) = 1 - \sum_{i=1}^N \frac{\lambda_i^{N-1} \exp(-\gamma/\lambda_i)}{\prod_{k \neq i} (\lambda_i - \lambda_k)}. \quad (7)$$

We refer to (7) as Lee's (CDF) formula. The effective diversity gain (EDG) is defined as the output of a diversity antenna improvement compared with that of a single ideal antenna at certain outage probability level, e.g. 1% [1]. The MRC EDG is,

$$EDG = \left. \frac{F^{-1}(\gamma)}{F_{ideal}^{-1}(\gamma)} \right|_{1\%} \quad (8)$$

where $(\cdot)^{-1}$ denotes functional inversion, and F_{ideal} is the CDF of output SNR of a single ideal antenna. For Rayleigh fading,

$$F_{ideal}(\gamma) = 1 - \exp(-\gamma). \quad (9)$$

The CDF of the MRC output SNR in Rayleigh fading is known for two cases:

- When all eigenvalues are different from each other it is given by (7);
- When all eigenvalues are equal, i.e. $\lambda_i = \lambda (i = 1 \dots M)$, it is given by [1]

$$F(\gamma) = 1 - \exp\left(-\frac{\gamma}{\lambda}\right) \sum_{i=1}^N \frac{(\frac{\gamma}{\lambda})^{i-1}}{(i-1)!}. \quad (10)$$

The CDF expressions with arbitrary equal eigenvalues are unknown in general and have to be approximated by empirical CDFs from measured channel samples. Since the EDG is determined from CDF consisting eigenvalues of the covariance matrix, we refer to this method of EDG calculation as covariance eigenvalue approach. Compared with traditional way of diversity measurement [14], the covariance-eigenvalue approach offers better accuracy with the same finite number of samples. Nevertheless, it is limited to MRC diversity in contrast to the generality of reading empirical CDF curves.

B. EDG Convergence in Distribution

We see from (7) that Lee's formula has an apparent singularity when any two eigenvalues of the covariance matrix are equal. Therefore, it is usually believed that Lee's formula will result in large numerical error when two eigenvalues are close to each other. In this paper, however, we show that Lee's formula converges to the true CDF when the eigenvalues approaches each other when the covariance matrix is estimated by the sample mean,

$$\hat{\mathbf{R}} = \frac{1}{M} \sum_{m=1}^M \mathbf{h}_m \mathbf{h}_m^H \quad (11)$$

where \mathbf{h}_m is the m th realization of random channel vector \mathbf{h} , and M is the number of realizations (or samples). We therefore refer to (11) as sample covariance matrix and its eigenvalues, $\hat{\lambda}_i (i = 1 \dots N)$, as sample eigenvalues.

To prove the convergence in distribution of EDG obtained using the covariance eigenvalue approach is equivalent to show that Lee's formula converges to the true CDF when the eigenvalues approach to each other.

First we consider the case when $N = 2$, and $\lambda_i \rightarrow \lambda (i = 1, 2)$. In this case, Lee's formula reduces to

$$F_{Lee}(\gamma) = 1 - \frac{\lambda_1 \exp(-\gamma/\lambda_1) - \lambda_2 \exp(-\gamma/\lambda_2)}{\lambda_1 - \lambda_2}. \quad (12)$$

The true CDF, i.e. the distribution of the MRC output of a two-port antenna with unity total embedded radiation efficiencies and no correlation, is

$$F(\gamma) = 1 - \exp\left(-\frac{\gamma}{\lambda}\right) \left(1 + \frac{\gamma}{\lambda}\right). \quad (13)$$

Namely, we need to show that $F_{Lee}(\gamma) \rightarrow F(\gamma)$ as $\lambda_i \rightarrow \lambda$.

Proof: Without loss of generality, let $\lambda_2 = \lambda$ and $\lambda_1 = \lambda + \varepsilon$ for any $\varepsilon > 0$ ($\lambda_i \rightarrow \lambda$ is equivalent to $\varepsilon \rightarrow 0$), and substitute these into (12),

$$F_{Lee}(\gamma) = 1 - \frac{\lambda}{\varepsilon} \left[\exp\left(-\frac{\gamma}{\lambda + \varepsilon}\right) - \exp\left(-\frac{\gamma}{\lambda}\right) \right] - \exp\left(-\frac{\gamma}{\lambda + \varepsilon}\right). \quad (14)$$

Denote $f(\lambda + \varepsilon) = \exp(-\gamma/\lambda + \varepsilon)$, using Taylor expansion to the first order,

$$f(\lambda + \varepsilon) = f(\lambda) + \frac{\gamma}{\lambda^2} \exp\left(-\frac{\gamma}{\lambda}\right) \varepsilon + o(\varepsilon) \quad (15)$$

where $o(\varepsilon) \rightarrow 0$ as $\varepsilon \rightarrow 0$. Substitute (15) into (14),

$$\begin{aligned} \lim_{\varepsilon \rightarrow 0} F_{Lee}(\gamma) &= \lim_{\varepsilon \rightarrow 0} \left\{ 1 - \frac{\lambda}{\varepsilon} \left[\frac{\gamma}{\lambda^2} \exp\left(-\frac{\gamma}{\lambda}\right) \varepsilon + o(\varepsilon) \right] \right. \\ &\quad \left. - \left[\exp\left(-\frac{\gamma}{\lambda}\right) + \frac{\gamma}{\lambda^2} \exp\left(-\frac{\gamma}{\lambda}\right) \varepsilon + o(\varepsilon) \right] \right\} \\ &= 1 - \frac{\gamma}{\lambda} \exp\left(-\frac{\gamma}{\lambda}\right) - \exp\left(-\frac{\gamma}{\lambda}\right) = F(\gamma). \end{aligned} \quad (16)$$

□

It is, however, difficult to prove that Lee's formula converges to the true CDF with arbitrary antenna ports (and therefore arbitrary number of equal eigenvalues) from CDF formula directly. We have to resort to the characteristic function for a more general proof.

It is self-evident from (5) that $\phi(z)$ converges as $\lambda_i \rightarrow \lambda$. Since $\phi(z)$ is the Fourier transform of the PDF of γ , to show that the limit of Lee's formula converges to the true CDF is equivalent to show that the convergence of $\phi(z)$.

Proof: Let F_i ($i = 1 \dots N$) be the CDF of γ when i eigenvalues of the covariance matrix are equal. Namely, F_1 denotes Lee's formula, F_{Lee} , and F_N represents the CDF of the MRC output with i.i.d. antenna branches. Due to bijection between the CDF and the characteristic function, there exists one $\phi_i(z)$ for each F_i uniquely. The Levy's continuity theorem [22] states that if $\phi_1(z)$ converges to $\phi_i(z)$ (that is continuous at 0), then F_1 converges to F_i . □

This is an immediate but general proof, yet it is rather abstract, for this reason, we would like to keep the proof for $N = 2$ case for the sake of better convergence illustration.

The convergence of Lee's formula to the true CDF means that the estimated MRC diversity gain using Lee's formula converges in distribution to its true value [22]. To further illustrate the convergence of the covariance-eigenvalue approach, we resort to simulations.

We first consider an ideal two-port diversity antenna with unity total embedded radiation efficiencies for both branches, and no correlation. The covariance matrix with perfect estimation \mathbf{R} is an identity matrix with equal eigenvalues of unity. In this case, there would have been singularity if we apply Lee's formula directly to \mathbf{R} . Nevertheless, in practice, the covariance matrices and eigenvalues in multipath fading environments are unknown, and have to be estimated from measurement samples. Thus $\hat{\lambda}_i$ deviate from λ_i with large probability. The question is

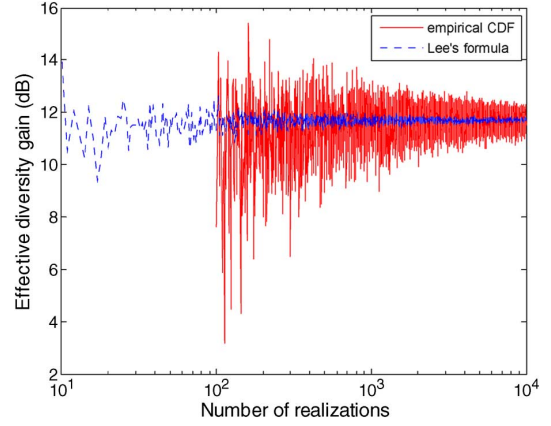


Fig. 1. Numerically simulated EDG as a function of number of realizations for ideal two-port antenna.

if there will be large numerical error using Lee's formula with finite number of realizations? To answer that, we generate i.i.d. complex Gaussian channel, represented by \mathbf{h}_w , with a Euclidean norm satisfying $E[\|\mathbf{h}_w\|_2^2] = N$, where $N = 2$ in this case. The channel seen by the diversity antenna can then be expressed as

$$\mathbf{h} = \mathbf{R}^{1/2} \mathbf{h}_w \quad (17)$$

where $\mathbf{R}^{1/2}$ is the Hermitian square root of \mathbf{R} , which is identity matrix \mathbf{I} in this case. The sample covariance matrix $\hat{\mathbf{R}}$ is estimated using (11), which deviates from \mathbf{I} (due to finite sample number M) with large probability.

Fig. 1 shows the EDGs (as a function of number of channel realizations) obtained using Lee's formula with sample eigenvalues $\hat{\lambda}_i$ against that obtained using the empirical CDF from channel realizations. The EDG converges to the true value, i.e., 11.7 dB, much faster than that based on using the empirical CDF. It is surprising to see that there is no noticeable error when the number of samples increases, knowing that the eigenvalues are estimated more accurately and therefore become very close to each other.

We then consider a three-port antenna with a covariance matrix

$$\mathbf{R} = \begin{bmatrix} 1 & 0.5 & 0.5 \\ 0.5 & 1 & 0.5 \\ 0.5 & 0.5 & 1 \end{bmatrix}, \quad (18)$$

so that two of the eigenvalues are equal ($\lambda_1 = 2$, $\lambda_2 = \lambda_3 = 0.5$). Repeat the same simulation procedure, the EDGs are calculated and shown in Fig. 2. It shows that the EDG obtained using Lee's formula with sample eigenvalues $\hat{\lambda}_i$ against that obtained using the empirical CDF. Similar simulation results are observed, i.e. EDG obtained using Lee's formula with sample eigenvalues not only converge to the true value but also converge much faster than that obtained from empirical CDF.

From both Fig. 1 and Fig. 2, it seems that the limit of Lee's formula converges to the true CDF when the eigenvalues converge to each other. In other words, the EDG obtained using covariance-eigenvalue approach converges in distribution to the true value. Lee's formula converges faster because the sample eigenvalues converge faster than the empirical CDF at

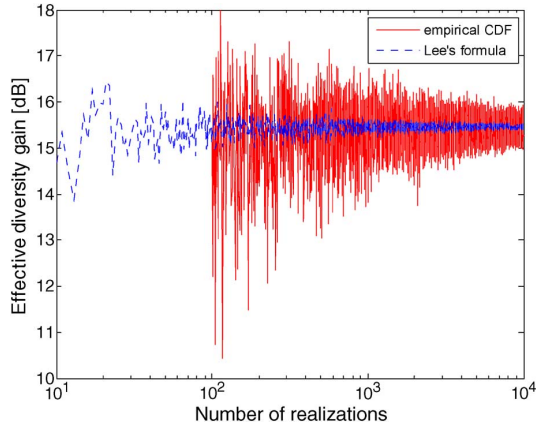


Fig. 2. Numerically simulated effective diversity gain as a function of number of realizations for three-port antenna with a uniform correlation of 0.5.

1% level. Note that, to be really sure to avoid singularities, one can add tiny marginal guards (say, “eps” in Matlab) between sample eigenvalues before substituting them into Lee’s formula. However, since $\hat{\lambda}_i$ deviate from λ_i with large probability and that Lee’s formula has a finite limit when the eigenvalues approach to each other, the singularity problem rarely happens in reverberation chamber measurements. Note that the simulations do not serve as a proof of the convergence but a confirmation of the rigid proof shown earlier in this subsection and an illustration of the convergence rate of the diversity gain estimates. Note also that the shown convergence of Lee’s formula does not mean that the covariance eigenvalue approach is numerically robust no matter what, since the probability that $\hat{\lambda}_i$ deviate from λ_i depends on the precision of the computer. This probability is arbitrarily close to 1 for modern computer with many precision bits and deviate from 1 for a digital signal processor (DSP) with finite bits. As a result, a large numerical error might be experienced when a real DSP is concerned. But for measurements with finite number of samples and a modern computer as the data processor, it is safe to use the covariance eigenvalue approach.

By now we have presented a fast-convergent approach (that works for arbitrary antennas) for determining MRC diversity gains from channel measurements. In the next section, we will present a general method for MIMO capacity calculation of arbitrary multi-port antennas based on their embedded far field functions and efficiencies.

III. FORMULATION FOR MIMO CAPACITY

We assume that the receiver has perfect channel state information, and that the transmitted power is equally allocated

among the transmit branches. The ergodic capacity of the multi-antenna system is [6]

$$C_{N_r \times N_t} = E \left\{ \log_2 \left[\det \left(\mathbf{I}_{N_t} + \frac{\gamma}{N_t} \mathbf{H}_{N_r \times N_t} \mathbf{H}_{N_r \times N_t}^H \right) \right] \right\} \quad (19)$$

where $\mathbf{H}_{N_r \times N_t}$ is the MIMO channel matrix, N_t and N_r are number of transmit and receive antennas, respectively. The subscripts in (19) will be dropped hereafter for notational convenience.

In order to focus on characterization of multi-port antennas, we assume the multi-port antenna under test is at the receive side and that the transmit antennas are ideal (i.e. with unity efficiency and no correlation). The ergodic capacity including overall antenna effects can be expressed as

$$\begin{aligned} C &= E \left\{ \log_2 \left[\det \left(\mathbf{I} + \frac{\gamma}{N_t} \left(\mathbf{R}^{\frac{1}{2}} \mathbf{H}_w \right) \left(\mathbf{R}^{\frac{1}{2}} \mathbf{H}_w \right)^H \right) \right] \right\} \\ &= E \left\{ \log_2 \left[\det \left(\mathbf{I} + \frac{\gamma}{N_t} \mathbf{R} \mathbf{H}_w \mathbf{H}_w^H \right) \right] \right\} \end{aligned} \quad (20)$$

where \mathbf{H}_w denotes the spatially white MIMO channel with i.i.d. complex Gaussian entries. \mathbf{H}_w is normalized so that its Frobenius norm satisfies $E[\|\mathbf{H}_w\|_F^2] = N_t N_r$. The physical meaning of this normalization is that every sub-channel (i.e. entry of the channel matrix) should have unity average channel gain.

The covariance matrix \mathbf{R} can be constructed by embedded radiation efficiencies at each antenna port and complex correlations between all the antenna ports. The embedded radiation efficiency can be measured in an anechoic chamber, while the complex correlation between m th and n th ports has to be determined from measured embedded far field functions at the corresponding ports [3], [7], (see (21) at the bottom of the page) where Ω is the solid angle of arrival, $\mathbf{g}_i (i = 1, \dots, N_r)$ is the embedded far field function (a column vector with elements representing for different polarizations) at the i th antenna port, and \mathbf{P}_{inc} is dyadic power angular spectrum of the incident waves. Note that in polarization-balanced isotropic scattering environments, e.g. reverberation chambers, $\mathbf{P}_{inc}(\Omega) = \mathbf{I}$.

Denote the efficiency vector consisting of all the total embedded radiation efficiencies and the correlation matrix as

$$\begin{aligned} \mathbf{e} &= [e_{emb1} \quad e_{emb2} \quad \cdots \quad e_{embN_r}]^T, \\ \Phi &= \begin{bmatrix} 1 & \rho_{12} & \cdots & \rho_{1N_r} \\ \rho_{12}^* & 1 & \cdots & \rho_{2N_r} \\ \vdots & \vdots & \ddots & \vdots \\ \rho_{1N_r}^* & \rho_{2N_r}^* & \cdots & 1 \end{bmatrix}. \end{aligned} \quad (22)$$

$$[\Phi]_{mn} = \frac{\iint_{4\pi} \mathbf{g}_m^H(\Omega) \mathbf{P}_{inc}(\Omega) \mathbf{g}_n(\Omega) d\Omega}{\sqrt{\iint_{4\pi} \mathbf{g}_m^H(\Omega) \mathbf{P}_{inc}(\Omega) \mathbf{g}_m(\Omega) d\Omega \cdot \iint_{4\pi} \mathbf{g}_n^H(\Omega) \mathbf{P}_{inc}(\Omega) \mathbf{g}_n(\Omega) d\Omega}} \quad (21)$$

The covariance matrix based on anechoic chamber measurements can be expressed as

$$\mathbf{R} = \mathbf{\Xi} \circ \mathbf{\Phi} \quad (23)$$

where $\mathbf{\Xi} = \sqrt{\mathbf{e}}\sqrt{\mathbf{e}^T}$, \circ denotes entry-wise product, the superscript T is the transpose operator, and $\sqrt{\cdot}$ is the entry-wise square root. The matrix $\mathbf{\Xi}$ can be expressed as (see (24) at the bottom of the page).

Since the embedded radiation efficiencies obtained from anechoic chamber measurements are based on measured embedded far field functions as well, we call this method embedded far field function method. For power-balanced multi-port antenna with a scalar embedded radiation efficiency of e_{emb} , \mathbf{R} becomes $e_{emb}\mathbf{\Phi}$, and (20) reduces to [15]

$$C = E \left\{ \log_2 \left[\det \left(\mathbf{I} + \frac{\gamma e_{emb}}{N_t} \mathbf{\Phi} \mathbf{H}_w \mathbf{H}_w^H \right) \right] \right\} \quad (25)$$

which is a special case of (20). Up to this point, we have extended the embedded far field function method in [15] to arbitrary multi-port antennas. Based on the generalized method, MIMO capacity of any multi-port antenna can be calculated based on measurements in an anechoic chamber.

IV. MEASUREMENTS AND RESULTS

A. Measurement in Reverberation Chamber

The reverberation chamber is basically a metal cavity with many excited modes which are stirred to create an isotropic Rayleigh-fading environment [24]. The Bluetest HP reverberation chamber is used in this work. It has a size of $1.75 \times 1.25 \times 1.8 \text{ m}^3$ and is provided with two plate stirrers, a turn-table platform (on which the antenna under test is mounted), and three wideband half bow-tie antennas (mounted on three orthogonal walls with different polarizations inside the chamber). We hereafter refer to these three antennas as wall antennas. Fig. 3 shows a drawing of the chamber.

In the measurements, the platform was moved to 20 positions spaced by 18° and at each platform position each of the two plates move simultaneously to 10 positions. At each stirrer position and for each of the three wall antennas a full frequency sweep was performed by a vector network analyzer (VNA). For diversity gain evaluations, we treat samples from the three wall antennas as the same random process; for MIMO capacity evaluations, we regard the wall antennas as independent transmit antennas. Therefore, for diversity evaluations there are 600 channel samples per frequency point, while for MIMO capacity evaluations there are 200 channel samples per frequency point.

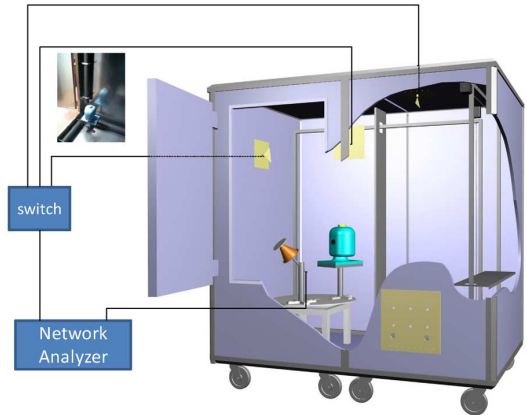


Fig. 3. Drawing of Bluetest reverberation chamber with two mechanical plate stirrers, a turn-table platform, and three wall antennas.

In order to improve measurement accuracy, the frequency stirring [25] is used. The frequency stirring technique, in principle, is to treat channel samples at different frequencies (within the frequency stirring bandwidth) as if they were from the same random process. Therefore, the frequency stirring bandwidth has to be carefully chosen so that more independent samples can be included without changing the channel statistics. Since the coherence bandwidth of the channel in the chamber for this setup is around 1–2 MHz [26], the frequency step is set to 1 MHz, and a 20-MHz frequency stirring is used. Therefore, eventually there are 12000 channel samples for diversity gain evaluations and 4000 channel samples for MIMO capacity evaluations.

The average power transfer function is measured using a reference antenna with known radiation efficiency. The reference level, P_{ref} , is obtained by dividing the average power level with the total radiation efficiency of the reference antenna. The measured diversity channel vector (MIMO channel matrix) $\mathbf{h}_{meas}(\mathbf{H}_{meas})$ is a function of frequency and stirrer positions. The normalized measured channels are

$$\begin{aligned} \mathbf{h} &= \mathbf{h}_{meas} / \sqrt{P_{ref}}, \\ \mathbf{H} &= \mathbf{H}_{meas} / \sqrt{P_{ref}}. \end{aligned} \quad (26)$$

Note that the reverberation chamber attenuation and the total radiation efficiency of the wall antennas are calibrated out by (26). Since the three wall antennas in the reverberation chamber are located far away from each other on three orthogonal walls, the correlations between them are negligible.

The covariance matrix at the receive side can be estimated using (11). Once the covariance matrix is calculated, the MRC

$$\mathbf{\Xi} = \begin{bmatrix} \frac{e_{emb1}}{\sqrt{e_{emb1}e_{emb2}}} & \sqrt{e_{emb1}e_{emb2}} & \cdots & \sqrt{e_{emb1}e_{embN_r}} \\ \sqrt{e_{emb1}e_{emb2}} & e_{emb2} & \cdots & \sqrt{e_{emb2}e_{embN_r}} \\ \vdots & \vdots & \ddots & \vdots \\ \sqrt{e_{emb1}e_{embN_r}} & \sqrt{e_{emb2}e_{embN_r}} & \cdots & e_{embN_r} \end{bmatrix}. \quad (24)$$

diversity gain can be readily obtained using the covariance eigenvalue approach. The ergodic MIMO capacity can be easily calculated using (19) with the (normalized) measured MIMO channel samples.

B. Measurement in Anechoic Chamber

Diversity and capacity measurements in an anechoic chamber are not as straightforward as those in the reverberation chamber in the sense that there is no random channel to measure in the anechoic chamber. For both diversity and capacity evaluations, we need to measure the embedded far field functions and embedded radiation efficiencies at every antenna port. In this paper, the embedded far field functions and efficiencies of the multi-port antenna under test were measured (with angular step of 1°) in the anechoic chamber at Technical University of Denmark (DTU), Lyngby, Denmark. During the measurement, the antenna under test is rotated by an azimuth positioner and the full-sphere near-field signal is measured on a regular grid by a dual-polarized probe located about 6 m away. The measured signal is then transformed to the far field using the spherical wave expansion and properly correcting for the probe characteristics.

For MRC diversity calculations, we need only to construct the covariance matrix \mathbf{R} (23), and then apply the covariance-eigenvalue approach directly. In that case, it is necessary to put tiny marginal guards (say, “eps” in Matlab) between the eigenvalues to avoid the singularity in Lee’s formula, because the anechoic chamber measurement is deterministic and therefore there is non-negligible probability that some eigenvalues are equal. For capacity evaluations, we can apply the embedded far field function method straightforwardly.

C. Eleven Antenna

The so-called Eleven antenna (see Fig. 4) is chosen as the antenna under test. It is a log-periodic multi-port antenna working from 2 to 13 GHz [27]. In this paper, the four ports for one polarization of Eleven antenna, shown in Fig. 5, are combined with wideband 180° hybrids to form two-port and three-port antennas as shown in Fig. 5 and Fig. 6, respectively. The ports of the two-port Eleven antenna are marked as ports P1 and P2 in Fig. 5. The ports of the three-port Eleven antenna are marked as ports P1, P2, and P3 in Fig. 6. In this paper, the two Eleven antenna configurations are measured from 2 to 8 GHz in both reverberation and anechoic chambers. The associate 180° hybrids have losses between 1.4 dB at 2 GHz and 3 dB at 8 GHz, which contribute the most ohmic losses.

Due to the symmetric property of Eleven antenna, we only measured the embedded far field function and total embedded radiation efficiency at port P1 for two-port Eleven antenna (see Fig. 5) and port P1 for three-port Eleven antenna (see Fig. 6), from 2 to 8 GHz with frequency step of 100 MHz. This simplification is necessary considering the time-consuming radiation pattern measurements in the anechoic chamber. As a result, for the two-port Eleven antenna, the embedded far field function at port P2 is obtained by rotating that of P1 by 180° . For the three-port Eleven antenna, the embedded far field function at P2 is obtained from that of P1 by imaging; and the embedded far field function at P3 is the same as that at P2 for the two-port

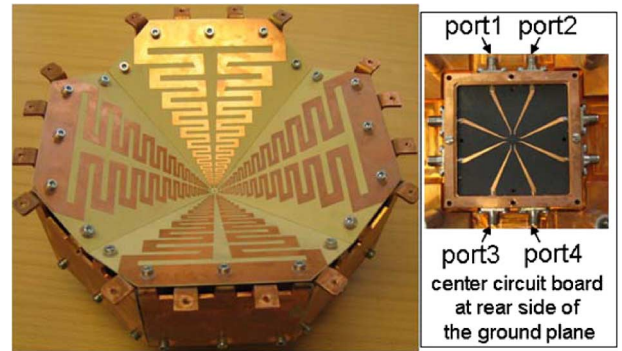


Fig. 4. Photos of front and back sides of Eleven antenna.

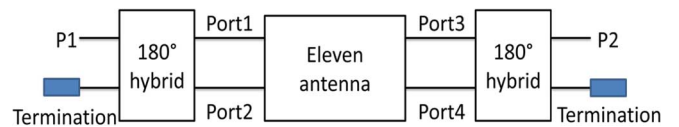


Fig. 5. Diagram of Eleven antenna with the four ports of one polarization combined to a two-port antenna.

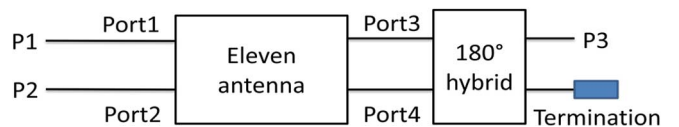


Fig. 6. Diagram of Eleven antenna with the four ports of one polarization combined to a three-port antenna.

Eleven antenna. Furthermore, the embedded radiation efficiency at P1 is the same as that at P2 for the two-port Eleven antenna; and that the total embedded radiation efficiency at P1 equals to that at P2 for the three-port Eleven antenna (with the total embedded radiation efficiency of P3 equal to that at P2 of the two-port Eleven antenna).

Note that the channel measurements in the reverberation chamber are much faster than the anechoic chamber measurements. We measured the channel samples at each port of both Eleven antennas with 1-MHz frequency step. The vector network analyzer (VNA) that is used for the reverberation chamber measurement can gather a maximum of 1601 samples per frequency sweep. Therefore, we divided the whole measurement frequency range into four sub-bands, each with a sub-bandwidth of 1.5 GHz, i.e. 2–3.5 GHz, 3.5–5 GHz, 5–6.5 GHz, and 6.5–8 GHz, and repeated the same measurement procedure over these four sub-bands.

D. Results and Discussions

Although correlations and embedded radiation efficiencies are only needed for diversity and capacity evaluations of anechoic chamber measurements (evaluations of reverberation chamber measurements are based on measured channel samples directly), it is still worthwhile to compare the measured embedded radiation efficiencies and correlations in both chambers, because they are also informative parameters for multi-port antenna characterizations. The embedded radiation efficiencies are readily obtained from anechoic chamber measurements; the measured correlation coefficients in the anechoic chamber can

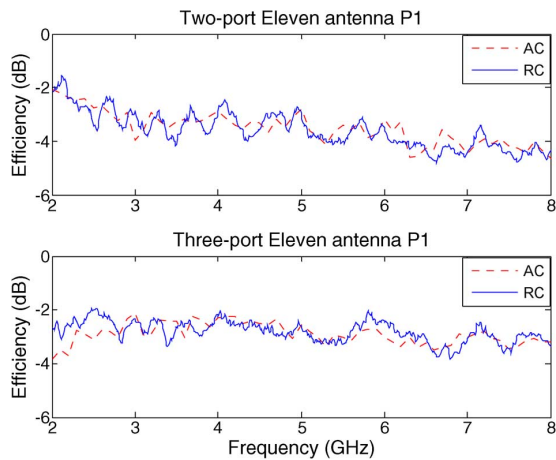


Fig. 7. Comparison of measured total embedded radiation efficiencies from anechoic chamber (AC) and reverberation chamber (RC).

be calculated using (21). The measured embedded radiation efficiencies in the reverberation chamber can be obtained by simply comparing the power levels of the sub-channels at corresponding antenna ports with the reference level P_{ref} (cf. Section IV-A). The measured correlation coefficients in the reverberation chamber can be obtained by

$$\hat{\rho}_{mn} = \frac{[\hat{\mathbf{R}}]_{mn}}{\sqrt{[\hat{\mathbf{R}}]_{mm}[\hat{\mathbf{R}}]_{nn}}} \quad (27)$$

with $\hat{\mathbf{R}}$ calculated by (11).

Due to the symmetry property of the Eleven antenna, we only compare the embedded radiation efficiencies at P1 of the two-port Eleven antenna, and at P1 of the three-port Eleven antenna. Fig. 7 shows the measured embedded radiation efficiencies of the Eleven antennas at both chambers. There are good agreements over most of the frequency range. Note that the used 180° hybrids are the dominate contributor to the total embedded radiation efficiency at P1 of the two-port Eleven antenna and that the mutual coupling is the main contributor to the embedded radiation efficiency at P1 of the three-port Eleven antenna.

Fig. 8 shows the measured correlation magnitudes from anechoic and reverberation chambers. There is excellent agreement for the correlation of the two-port Eleven antenna. Although the agreements of correlations between different ports of the three-port Eleven antenna is not as good as that, their agreement is acceptable, since it is difficult to measure small correlation accurately.

The MRC diversity gains of the two-port and three-port Eleven antennas based on reverberation and anechoic chamber measurements are shown in Fig. 9, as a function of frequency. As expected, the diversity gains measured from both chambers agree with each other well over most of the frequency range. Similarly, the ergodic capacities of the two-port and three-port Eleven antennas are calculated at 10-dB SNR and shown in Fig. 10, as a function of frequency. Again good agreements are observed. Note that for better illustration, the corresponding diversity gain and ergodic capacity values of ideal antennas (with i.i.d. channels) are not plotted in the same figures. Since the ideal case values are independent of frequency, we give a

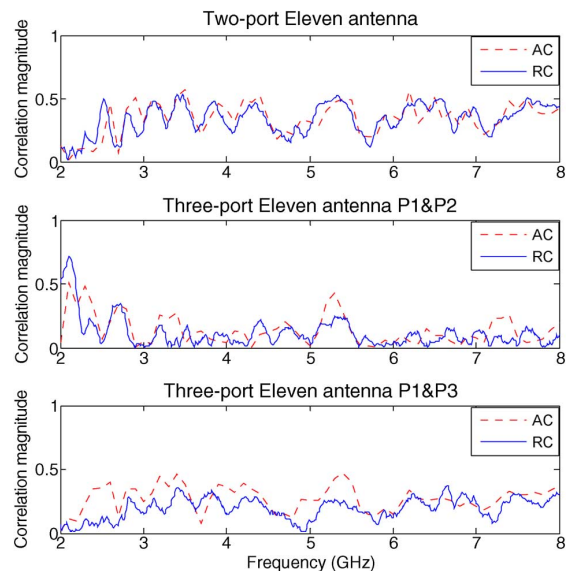


Fig. 8. Comparison of measured correlation magnitudes from anechoic chamber (AC) and reverberation chamber (RC).

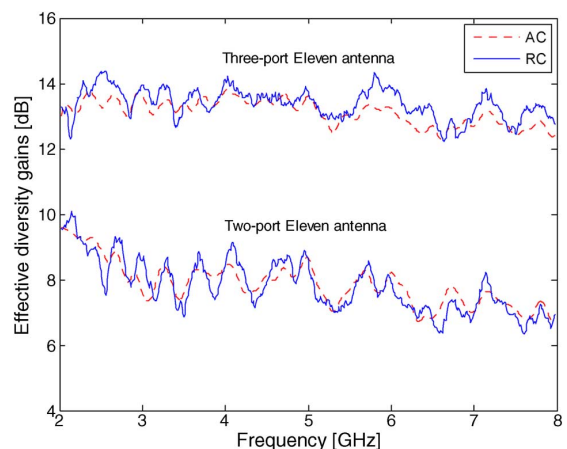


Fig. 9. Comparison of MRC EDG of two-port and three-port Eleven antennas from anechoic chamber (AC) and reverberation chamber (RC). The corresponding ideal two-port and three-port antenna (with i.i.d. channels) have EDGs of 11.7 and 16.4 dB respectively.

single value for each case in the captions of Fig. 9 and Fig. 10 respectively.

The ergodic capacity is the average of the instantaneous capacity. Since the instantaneous capacity depends on the channel state, it is itself a random variable. Therefore, a closer capacity evaluation would be comparison of the empirical CDF of the capacity estimates. Fig. 11 and Fig. 12 show the empirical CDFs of the capacities of the two-port and three-port Eleven antennas, respectively, at a few frequencies with 10-dB SNR. As expected, there are reasonable agreements between the empirical CDFs. For comparison, we also plotted the empirical CDF of the corresponding ideal antennas (with i.i.d. channels). As mentioned earlier, the capacity (and EDG) degradation is mainly due to the ohmic loss introduced by the 180° hybrids rather than the antenna itself. For a closer look at the antenna effects on diversity gains and ergodic capacities, we calculated for the two-port Eleven antenna the degradation contributions of antenna

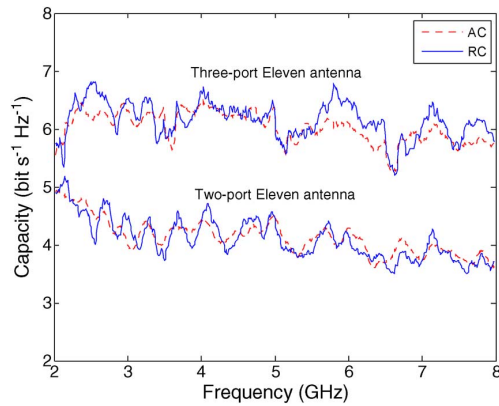


Fig. 10. Comparison of ergodic capacities of two-port and three-port Eleven antennas from anechoic chamber (AC) and reverberation chamber (RC), both at SNR of 10 dB. The corresponding ideal two-port and three-port antennas (with i.i.d. channels) have ergodic capacities of 6.0 and 8.2 bps/Hz respectively.

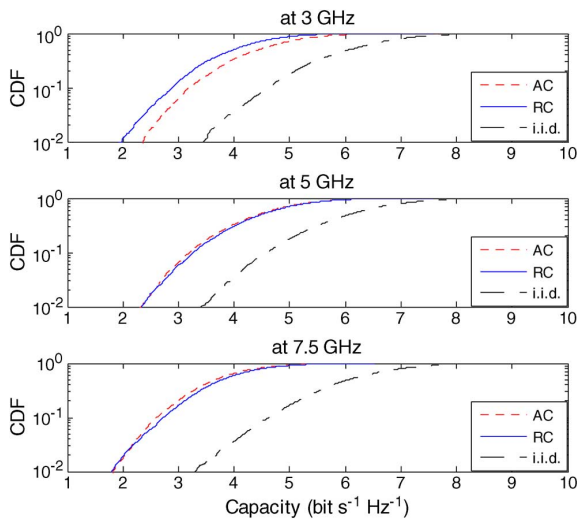


Fig. 11. Comparison of capacity CDF of two-port Eleven antennas from anechoic chamber (AC) and reverberation chamber (RC), both at SNR of 10 dB.

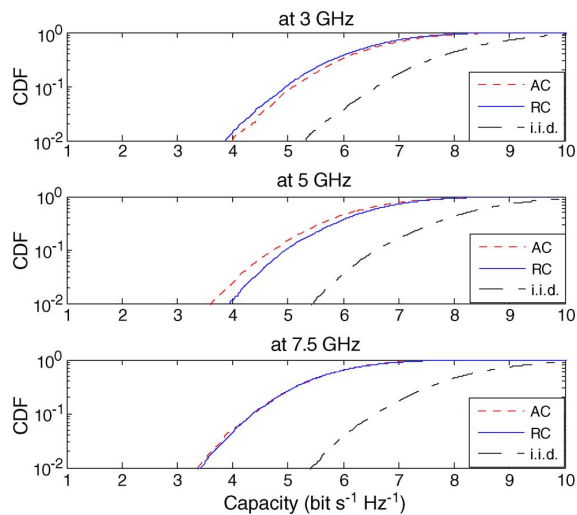


Fig. 12. Comparison of capacity CDF of three-port Eleven antenna from anechoic chamber (AC) and reverberation chamber (RC), both at SNR of 10 dB.

efficiencies and correlations respectively, as shown in Table I and Table II, where the efficiency and correlation are obtained

TABLE I
EFFECTIVE DIVERSITY GAINS (EDG) OF TWO-PORT ELEVEN ANTENNA WITH EFFICIENCY AND CORRELATION CONTRIBUTIONS

	3 GHz	5 GHz	7.5 GHz
Ideal EDG (dB)	11.7	11.7	11.7
Efficiency (dB)	-4.0	-2.8	-4.2
EDG with only efficiency (dB)	7.7	8.9	7.5
Correlation magnitude	0.31	0.31	0.41
EDG with only correlations (dB)	11.5	11.5	11.3
EDG with both efficiency and correlation (dB)	7.5	8.6	7.1

TABLE II
ERGODIC CAPACITIES OF TWO-PORT ELEVEN ANTENNA WITH EFFICIENCY AND CORRELATION CONTRIBUTIONS AT 10-dB SNR

	3 GHz	5 GHz	7.5 GHz
Ideal capacity (bps/Hz)	6.04	6.04	6.04
Efficiency (dB)	-4.0	-2.8	-4.2
Capacity with only efficiencies (bps/Hz)	4.03	4.57	3.92
Correlation magnitude	0.31	0.31	0.41
Capacity with only correlations (bps/Hz)	5.94	5.94	5.86
Capacity with both efficiencies and correlations (bps/Hz)	3.95	4.49	3.83

based on the anechoic chamber measurement and that the EDG and capacity values are calculated using the covariance eigenvalue approach and embedded far field function method (with 4000 numerically generated random channel samples), respectively. The effects of antenna efficiency and correlation on diversity gain and capacity for the three-port Eleven antenna are quite similar, i.e., the efficiency is the major contribution to both degradations of diversity gain and ergodic capacity, given the fact the correlation magnitude is below 0.5. Note that the antenna efficiency is mainly due to the ohmic losses in the 180° hybrids.

From both diversity and capacity comparisons between reverberation and anechoic chamber measurements, it is safe to conclude that both chambers can give approximately the same results with reasonable accuracies. It would be impractically time consuming and expensive to determine the diversity and capacity measurement uncertainties by repeating the measurements many times. Using Monte Carlo simulations, together with known antenna radiation efficiency uncertainties in both chambers, it is shown that the measurement efficiency uncertainty is the major uncertainty contributor [28]. The uncertainty of efficiencies measured in the Bluetest reverberation chamber is normally smaller than a standard deviation (STD) of 0.5 dB [29], whereas the anechoic chamber at DTU has a STD of 0.2 dB for Eleven antenna measurements [30]. Thus the anechoic chamber measurement is more accurate.

For the reverberation chamber measurement, we actually used a four-port VNA to sample channels in reverberation chamber. Therefore we can measure up to three antenna ports in one run. As a result, the measurement times for the two-port and three-port Eleven antenna are almost the same, i.e. about 1.5 hours. The times used to measure embedded far field functions is around 10 hours in the anechoic chamber for each port. In principle, one needs 20 hours for measuring the two-port Eleven antenna, and 30 hours for measuring the three-port Eleven antenna. Knowing the symmetric property of Eleven antenna, we only measured the embedded far field function at port P1 for the two-port Eleven antenna (see Fig. 5), and port P1 for the three-port Eleven antenna (see Fig. 6), as explained in Section IV-C. Note that, in principle, the embedded far field function and embedded radiation efficiency at each antenna port must be measured in an anechoic chamber for general multi-port antennas that do not have the symmetric property. This means that the measurement time in the anechoic chamber increases with a factor of antenna port number, in general, for arbitrary multi-port antennas. Given the fact that both chambers offer reasonable accuracies and that the embedded far field function method is much more time-consuming compared with the straightforward capacity calculation based on measured channel samples, the reverberation chamber seems more suitable for evaluations of multi-port antennas.

V. CONCLUSION

We presented the covariance eigenvalue approach for MRC diversity gain calculations, which is very suitable for reverberation chamber measurements. We showed that this approach is generally valid for practical measurements of arbitrary multi-port antennas, despite the mathematical singularity in its CDF formula. We also showed how to apply this approach to anechoic chamber measurements. We presented the embedded far field function method for capacity evaluations based on anechoic chamber measurements for arbitrary multi-port antennas. Based on it, the ergodic MIMO capacity can be calculated based on embedded far field functions and embedded radiation efficiencies measured in an anechoic chamber. We compared reverberation chamber measurements with that of an anechoic chamber using the covariance-eigenvalue approach for diversity gain evaluations and the embedded far field function method for capacity evaluations. Good agreements between measured MRC diversity gains and MIMO capacities in both chambers are observed (despite of small discrepancies), meaning both chambers give acceptable measurement accuracy. Nevertheless, it is shown that MRC diversity gain and MIMO capacity can be readily calculated from direct channel measurements in a reverberation chamber and that the reverberation chamber measurement is much faster than that of an anechoic chamber.

REFERENCES

- [1] M. Schwartz, W. R. Bennett, and S. Stein, *Communication Systems and Techniques*. Piscataway, NJ: IEEE press, 1996.
- [2] W. C. Y. Lee, "Mutual coupling effect on maximum-ratio diversity combiners and application to mobile ratio," *IEEE Trans. Commun. Technol.*, vol. COM-18, pp. 779–791, Dec. 1970.
- [3] R. G. Vaughan and J. B. Andersen, "Antenna diversity in mobile communications," *IEEE Trans. Vehic. Technol.*, vol. 36, no. 4, pp. 149–172, Nov. 1987.
- [4] O. Norklit, P. D. Teal, and R. G. Vaughan, "Measurement and evaluation of multi-antenna handsets in indoor mobile communication," *IEEE Trans. Antennas Propag.*, vol. 49, no. 3, pp. 429–437, Mar. 2001.
- [5] V. Plicanic, B. K. Lau, A. Derneryd, and Z. Ying, "Actual diversity performance of a multiband diversity antenna with hand and head effects," *IEEE Trans. Antennas Propag.*, vol. 57, no. 5, pp. 1547–1556, May 2009.
- [6] C. J. Foschini, "Layered space-time architecture for wireless communication in a fading environment when using multi-element antennas," *Bell Labs Tech. J.*, vol. 1, pp. 41–59, 1996.
- [7] B. T. Quist and M. A. Jensen, "Optimal antenna radiation characteristics for diversity and MIMO systems," *IEEE Trans. Antennas Propag.*, vol. 57, no. 11, pp. 3474–3481, Nov. 2009.
- [8] J. W. Wallace and M. A. Jensen, "Mutual coupling in MIMO wireless systems: A rigorous network theory analysis," *IEEE Trans. Wireless Commun.*, vol. 3, no. 4, pp. 1317–1325, July 2004.
- [9] Y. Fei, Y. Fan, B. K. Lau, and J. S. Thompson, "Optimal single-port matching impedance for capacity maximization in compact MIMO arrays," *IEEE Trans. Antennas Propag.*, vol. 56, no. 11, pp. 3566–3575, Nov. 2008.
- [10] E. Genender, C. L. Holloway, K. A. Remley, J. M. Ladbury, G. Koepke, and H. Garbe, "Simulating the multipath channel with a reverberation chamber: Application to bit error rate measurements," *IEEE Trans. Electromagn. Compat.*, vol. 52, pp. 766–777, 2010.
- [11] G. Ferrara, M. Migliaccio, and A. Sorrentino, "Characterization of GSM non-line-of-sight propagation channels generated in a reverberating chamber by using bit error rates," *IEEE Trans. Electromagn. Compat.*, vol. 49, no. 3, pp. 467–473, Aug. 2007.
- [12] P.-S. Kildal, X. Chen, C. Orlenius, M. Franzén, and C. Lötbäck Patané, "Characterization of reverberation chambers for OTA measurements of wireless devices: Physical formulations of channel matrix and new uncertainty formula," *IEEE Trans. Antennas Propag.*, vol. 60, no. 8, pp. 3875–3891, 2012.
- [13] P.-S. Kildal and K. Rosengren, "Correlation and capacity of MIMO systems and mutual coupling, radiation efficiency and diversity gain of their antennas: Simulations and measurements in reverberation chamber," *IEEE Commun. Mag.*, vol. 42, no. 12, pp. 102–112, Dec. 2004.
- [14] X. Chen, P.-S. Kildal, and J. Carlsson, "Fast converging measurement of MRC diversity gain in reverberation chamber using covariance-eigenvalue approach," *IEICE Trans. Electron.*, vol. E94-C, no. 10, pp. 1657–1660, Oct. 2011.
- [15] X. Chen, P.-S. Kildal, J. Carlsson, and J. Yang, "Comparison of ergodic capacities from wideband MIMO antenna measurements in reverberation chamber and anechoic chamber," *IEEE Antennas Wireless Propag. Lett.*, vol. 10, pp. 446–449, 2011.
- [16] X. Chen, P.-S. Kildal, J. Yang, and J. Carlsson, "Capacity characterization of Eleven antenna in different configurations for MIMO applications using reverberation chamber," in *Proc. 6th Eur. Conf. Antennas Propag.*, Prague, Mar. 26–30, 2012, pp. 1571–1575.
- [17] J. F. Valdes, M. A. Fernandez, A. M. Gonzalez, and D. A. Hernandez, "The influence of efficiency on receive diversity and MIMO capacity for Rayleigh-fading channels," *IEEE Trans. Antennas Propag.*, vol. 56, no. 5, pp. 1444–1450, May. 2008.
- [18] L. Garcia-Garcia, B. Lindmark, N. Jalden, and C. Orlenius, "MIMO capacity of antenna arrays evaluated using radio channel measurements, reverberation chamber and radiation patterns," *IET Microw. Antennas Propag.*, vol. 1, pp. 1160–1169, 2007.
- [19] P.-S. Kildal, A. Hussain, X. Chen, C. Orlenius, A. Skårbratt, J. Asberg, T. Svensson, and T. Eriksson, "Threshold receiver model for throughput of wireless devices with MIMO and frequency diversity measured in reverberation chamber," *IEEE Antennas Wireless Propag. Lett.*, vol. 10, pp. 1201–1204, 2011.
- [20] P.-S. Kildal, C. Orlenius, and J. Carlsson, "OTA testing in multipath of antennas and wireless devices with MIMO and OFDM," *Proc. IEEE*, vol. 100, no. 7, pp. 2145–2157, Jul. 2012.
- [21] K. A. Remley, H. Fielitz, C. L. Holloway, Q. Zhang, Q. Wu, and D. W. Matolak, "Simulation of a MIMO system in a reverberation chamber," in *Proc. IEEE EMC Symp.*, Aug. 2011.
- [22] D. Williams, *Probability With Martingales*. Cambridge, U.K.: Cambridge Univ. Press, 1991.
- [23] G. L. Turin, "The characteristics function of Hermitian quadratic forms in complex normal variables," *Biometrika*, vol. 47, pp. 199–201, 1960.
- [24] J. G. Kostas and B. Boverie, "Statistical model for a mode-stirred chamber," *IEEE Trans. Electromagn. Compat.*, vol. 33, no. 4, pp. 366–370, Nov. 1991.

- [25] D. A. Hill, "Electronic mode stirring for reverberation chamber," *IEEE Trans. Electromagn. Compat.*, vol. 36, no. 4, pp. 294–299, Nov. 1994.
- [26] X. Chen, P.-S. Kildal, C. Orlenius, and J. Carlsson, "Channel sounding of loaded reverberation chamber for over-the-air testing of wireless devices—Coherence bandwidth and delay spread versus average mode bandwidth," *IEEE Antennas Wireless Propag. Lett.*, vol. 8, pp. 678–681, 2009.
- [27] J. Yang, M. Pantaleev, P.-S. Kildal, Y. Karadikar, L. Helldner, B. Klein, N. Wadefalk, and C. Beaudoin, "Cryogenic 2–13 GHz eleven feed for reflector antennas in future wideband radio telescopes," *IEEE Trans. Antennas Propag.*, vol. 59, no. 6, pp. 1918–1934, Jun. 2011.
- [28] X. Chen, P.-S. Kildal, and J. Carlsson, "Measurement uncertainties of capacities of multi-antenna system in anechoic chamber and reverberation chamber," in *Proc. 8th Int. Symp. Wireless Commun. Systems (ISWCS'11)*, Aachen, Germany, Nov. 2011, pp. 216–220.
- [29] P.-S. Kildal and C. Carlsson, TCP of 20 Mobile Phones Measured in Reverberation Chamber 2002, Bluetest Tech. Rep.
- [30] S. Pivnenko, Private Communications Technical Univ. Denmark. Lyngby, Denmark, 2011.



Xiaoming Chen received the B.Sc. degree from Northwestern Polytechnical University, Xi'an, China, in 2006, and the M.Sc. and Ph.D. degrees from Chalmers University of Technology, Gothenburg, Sweden, in 2007 and 2012, respectively.

He is now a Research Associate in the Department Of Signals And Systems, Chalmers University of Technology. His current research areas include reverberation chamber measurements, multi-antenna channel characterization, and statistical Electromagnetics. He is a reviewer for the IEEE TRANSACTIONS

ON ANTENNAS AND PROPAGATION, IEEE TRANSACTIONS ON WIRELESS COMMUNICATIONS, IEEE TRANSACTIONS ON VEHICULAR TECHNOLOGY, and IEEE TRANSACTIONS ON ELECTROMAGNETIC COMPATIBILITY.



Per-Simon Kildal (M'76–SM'81–F'95) is a Professor of antennas at Chalmers University of Technology in Gothenburg, Sweden since 1989, where he heads the Antenna group. His main tasks are to lead and supervise research and education within antenna systems. Eighteen people have received the Ph.D. degree from him. He has authored more than 120 articles in scientific journals; concerning antenna theory, analysis, design and measurements, two of which was awarded best paper awards by IEEE (1985 R.W.P. King Award and

1991 Schelkunoff Prize Paper Award). In 2011, he was awarded the prestigious Distinguished Achievements Award from the IEEE Antennas and Propagation Society. He has done the electrical design of the 40 m × 120 m cylindrical reflector antenna and line feed of the EISCAT scientific organization, and the dual-reflector Gregorian feed of the 300 m ∅ radio telescope in Arecibo. He is the inventor behind technologies such as dipole with beam forming ring, the hat antenna, and the eleven feed. He was the first to introduce the reverberation chamber as an accurate measurement instrument tool for over-the-air (OTA)

characterization of small antennas and wireless terminals for use in multipath environments with fading. He is also the originator of the concept of soft and hard surfaces from 1988, today being regarded as the first metamaterials concept. This concept is the basis of his newest and most fundamental invention, the gap waveguide technology. His research is innovative and industrially oriented, and has resulted in several patents and related spinoff companies, the most known being Bluetest AB. He organizes and lectures in courses within the European School of Antenna (ESoA, <http://www.antennasvce.org>). His textbook *Foundations of Antennas—A Unified Approach* (Lund, Sweden: Studentlitteratur, 2000) was well received, and is now in the process of being revised.



Jan Carlsson (M'98) was born in Sweden on May 6, 1962. He received the M.S.E.E. and Ph.D. degrees from Chalmers University of Technology, Gothenburg, Sweden, in 1986 and 1998, respectively.

From 1986 to 1990, he was an Electromagnetic Compatibility (EMC) Engineer with Ericsson Radar Electronics AB, Mölndal, Sweden. He is currently the Head of Research in the EMC Department, SP Technical Research Institute of Sweden, Borås, Sweden. He is also an Adjunct Professor of computational electromagnetics in the Department of

Signals and Systems, Chalmers University of Technology. His current research interests include the area of computation techniques for electromagnetic problems, especially for applications in EMC and antennas. Since 2009 he is assistant centre manager of Chase, Chalmers Antenna Systems VINN EXcellence Centre at Chalmers University of Technology. He is the coauthor of the *EMMA Handbook* (EMC handbook issued by the Swedish Defence Materiel Administration).

Dr. Carlsson is a Member of the Swedish National Committee for Radio Science (SNRV), Section E. He has been a reviewer for several international journals. From 2002–2004 he was the Chairman of the Swedish IEEE EMC Chapter.



Jian Yang (M'02–SM'10) received the B.S. degree from the Nanjing University of Science and Technology, Nanjing, China, in 1982 and the M.S. degree from the Nanjing Research Center of Electronic Engineering, Nanjing, China, in 1985, both in electrical engineering, and the Swedish Licentiate and Ph.D. degrees from the Chalmers University of Technology, Gothenburg, Sweden, in 1998 and 2001, respectively.

From 1985 to 1996, he was with the Nanjing Research Institute of Electronics Technology, Nanjing, China, as a Senior Engineer. From 1999 to 2005, he was with the Department of Electromagnetics, Chalmers University of Technology, as a Research Engineer. During 2005 and 2006, he was with COMHAT AB as a Senior Engineer. Since 2006, he has been an Assistant Professor in the Department of Signals and Systems, Chalmers University of Technology. Since 2010, he has been titled as Associate Professor. His research interests include ultra-wideband antennas and UWB feeds for reflector antennas, UWB radar systems, UWB antennas in near-field sensing applications, hat-fed antennas, reflector antennas, radome design, and computational electromagnetics.